Desalination and Water Treatment
www.deswater.com
doi: 10.1080/19443994.2015.1025432

57 (2016) 6594–6603
March

Taylor & Francis
Taylor & Francis Group

Synthesis and characterization of mackinawite nanocrystals (FeS_m) and their application in recovery of aqueous Hg(II) solution

Saad M. Alshehri*, Ali Aldalbahi, Tansir Ahamad, Norah Alhokbany

Department of Chemistry, College of Science, King Saud University, P.O. Box 2455, Riyadh 11451, Kingdom of Saudi Arabia, Tel. +966 1 4675971; Fax: +966 1 4674018; email: alshehri@ksu.edu.sa (S.M. Alshehri)

Received 25 November 2013; Accepted 11 January 2015

ABSTRACT

Stabilized FeS_m (Mackinawite) nanocrystals have been synthesized by hydrothermal treatment of single precursor polymer metal complex. The polymer metal complex was prepared by the reaction of thiourea-formaldehyde resin with metal Fe(II) ion. The synthesized FeS_m nanocrystals were characterized by X-ray spectrometry and electronic microscopy. The transmission electron microscopy micrographs showed needle shaped nanocrystals and the thickness and length of these nanocrystals were found to be 12 ± 3 and 120 ± 5 nm, respectively. The lattice fringes in the HRTEM images, with *d*-spacing 0.521 ± 0.005 nm very close to (0 0 1) plane of mackinawite nature. The interaction between aqueous Hg(II) and synthetic FeS_m was studied via batch sorption experiments. The maximum absorption capacity of FeS_m has been found with 0.001:0.08 M ratio of Hg(II) and FeS_m, while the minimum absorption capacity was found with 0.001:0.005 M ratio of Hg(II) and FeS_m and removed only 60% of Hg(II) from aqueous solution. Batch studies revealed that FeS_m nanocrystals were effectively remove Hg(II) from aqueous solution along a broad pH range.

Keywords: Mackinawite; Polymer metal complex; Nanocrystals; Sorption

1. Introduction

Contamination of water due to heavy metals is caused by several sources such as petrochemical industries, acid mine drainage, electro-painting, and agricultural sources such as fertilizers and fungicidal sprays, or by natural source such as volcanic activity [1,2]. Mercury and its compounds are cumulative toxins and in small quantities are hazardous to human health [3]. WHO report the major effects of mercury poisoning manifest as neurological and renal disturbances as it can easily pass the blood brain barrier and affect on the brain. High concentration of Hg(II) cause impairment of pulmonary function and kidney, chest pain, and dyspnoea [4–7]. Although much work has been done on the removal of Hg from water and wastewater including chemical precipitation, conventional coagulation, lime softening, reverse osmosis, ion-exchange, and activated carbon adsorption, little attention was paid to simultaneously removing them using a relatively effective and cheap process [8–10]. Sulfide minerals have great thermodynamic potential for Hg(II) immobilization through adsorption or co-precipitation [11]. The most common iron sulfide minerals are pyrite, pyrrhotite, and meckinawite. Adsorption is a conventional, but efficient technique to remove mercury from aqueous solutions using highly porous materials with adequate surface area.

*Corresponding author.

Iron sulfide has also been shown to exchange its Fe(II) with Hg(II) to form HgS, which is extremely stable ($K_{sp} = 2 \times 10^{-53}$) [12]. Thus, developing an adsorbent with large surface area and small diffusion resistance is of great significance in absorption technology. Nanocrystalline materials represent a bridge between molecules and solid state and exhibit properties that are unique to solve environmental problems, such as accelerating the coagulation of sewage, removing radionuclides, adsorption of organic dyes, and remediation of contaminated soils [13,14]. Nanotechnology also offers new and efficient ways for removal of organic and inorganic pollutants, especially in water, because of the high surface/volume ratio of nanomaterials [15,16]. Among these, iron-based nanomaterials as solid phase extractors were promising in the removal of pollutants, because they are easily removed from a water solution. Mackinawite is a widely reported iron sulfide synthesized for those environmental remediation studies in the laboratory. This compound is prepared by simply mixing Fe^{2+}-containing and S^{2-}-containing salts together under anaerobic condition. These sulfide-based nanoparticles have been researched specifically to eliminate the contaminations of mercury (Hg) and arsenic (As) in water and soil/sediment by providing sulfide (S^{-2}) ligands and/or coordination surfaces. As a matter of fact, reduced sulfur (S^{2-}) has been regarded as a stabilizer/sink of heavy metals in the reduced environment such as in the sediments or water-logged soils by forming highly insoluble metal sulfides [17,18]. It is in high demand to develop novel nanomaterial sorbents with simple preparation process, low price, high efficiency, good stability, and reusability for mercury removal. If smaller sulfide (S^{-2}) containing particles are added, the removal mechanism will include sorption and surface reaction. Nano-scale iron sulfide particles have been produced microbially or abiotically and they have been applied to removal of metal ions. Keeping these fact in our mind, in the present study, we prepared easily and economically FeS_m nanoparticles and used to recover mercury from aqueous solution. The synthesized nanoparticles and adsorbed mercury (sediment) were characterized using transmission electron microscopy (TEM), HRTEM, energy-dispersive spectroscopy (EDS or EDX), selected area electron diffraction (SAED), and XRD technique.

2. Experimental

2.1. Materials

All the chemicals used in this study were analytical grade. $FeCl_2$, $HgCl_2$, thiourea, formaldehyde, triethenol amine were purchased from Sigma-Aldrich. All aqueous solutions were prepared with the deoxygenated water that had been prepared by purging Milli-Q water with high purity N_2 for at least 30 min. Thiourea formaldehyde resin were prepared as reported methods [19]. At room temperature, Thiourea (0.1 mol) and formaldehyde (0.2 mol) were mixed in a 250 mL three-neck round-bottomed flask connected to a reflux condenser and equipped with a mechanical stirrer; the pH of solution was adjusted to 8–9 with TEA and temperature was kept at 60–70˚C for 3 h, then the thiourea-formaldehyde resin solution was obtained as shown in Scheme 1.

2.2. Characterization

The synthesized nanocrystals FeS_m and sediments (FeS_m/HgS) were characterized by X-ray powder diffraction (XRPD) PAN analytical X'Pert Pro X-ray diffractometer with Cu Kα ($\lambda = 1.54$ Å) was used to study). TEM images and the corresponding SAED patterns were carried out on a (FESEM-JSM 7600F) electron microscope. For TEM observation, the synthesized products and sediments were ultrasonically dispersed in ethanol, and a drop of the suspension was placed on a Cu grid coated with carbon film. The specific surface area of N_2-dried mackinawite was measured following the multipoint N_2-BET adsorption method. Approximately 1.2 g samples were loaded in the sample holder and degassed for 12 h at 100˚C under 0.035 mmHg and specific surface area of FeS_m nanocrystal was found to be 120 m^2/g.

2.3. Synthesis of FeS_m nanocrystals (mackinawite)

FeS_m nanocrystals were prepared by mixing $FeCl_2$ (6 g mol) dissolved in a beaker containing 10 mL of distilled water and then mixed with 10 g of thiourea formaldehyde resin to yield a black homogeneous thiourea-formaldehyde-Fe(II) complex solution; it was transferred into a 35-mL Q-tube reactor, which contained 15 mL of distilled water. The Q-tube was maintained at 170˚C for 5 h. After the mixture cooled naturally to room temperature, the black precipitate was washed with deoxygenated water and ethanol for several times, and the final product was dried in a vacuum at 60˚C for 4 h. The resulting sample was kept in sealed vials or vacuum desiccators to minimize oxygen exposure during the transfer.

2.4. Absorption studies and analysis

Hg(II) absorption studies were carried out by rotating 0.1–0.005 M of FeS_m nanocrystals with a stock

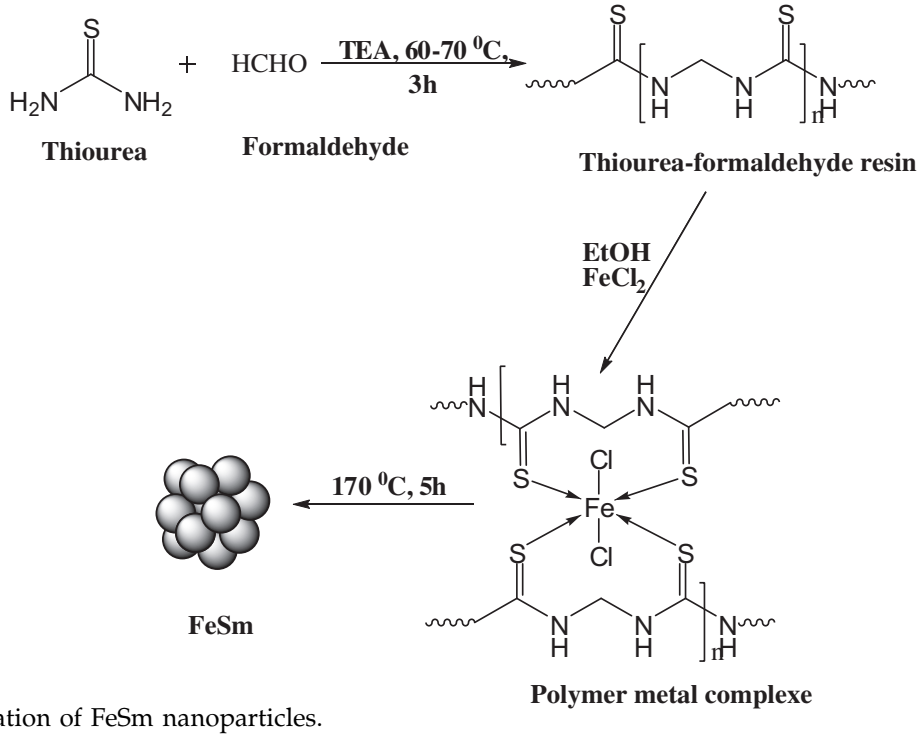

Scheme 1. Prepration of FeSm nanoparticles.

solution of $HgCl_2$ with initial Hg(II) concentration 0.01–0.0005 M in a 25 ml Teflon vials. All the solutions were prepared using deoxygenated mili Q water by purging N_2, and anaerobic condition were maintained by conducting the experiments inside a glove box under the flow of N_2. The pH of the solution was adjusted between 4 and 12 using N_2 purged 0.05 M HCl and 0.05 M NaOH solutions. The vials were rotated at 6,000 rpm for 25 min at room temperature and the supernatant was filtered through a 22 μm micro disk syringe filter membrane to separate the Hg (II). Although the pore size of the membrane is larger than the nanoparticles, the filtration was able to catch more than 90% of the nanoparticles measured as soluble Fe(II) [20]. The filtrates were acidified with 10% (w/w) HNO_3. Dissolved Hg concentration in the acidified solution was measured by cold vapor atomic absorption spectroscopy using atomic absorption spectrometer (varian spectra AA 220 FS) with $SnCl_2$ as reducing agent. Mercury sample, preparation, preservation, and analysis were conduct similar to the US. EPA method 1631. Before analysis, all the samples were preserved and oxidized with 1% BrCl followed by 1% hydroxylamine hydrochloride to destroy the residual BrCl. The amount of adsorbed Hg(II) per unit mass of FeS_m nanocrystals q_e in (mg Hg(II)/g FeS_m) was determined by using the following equations:

$$q_e = \frac{(C_0 - C_e)V}{M} \quad (1)$$

$$\text{Sorption efficiency } (\%) = \frac{(C_0 - C_e)}{C_0} \times 100 \quad (2)$$

where C_0 and C_e (mg/L) are the concentration of Hg (II) at initial and equilibrium, respectively, M is the mass of FeS_m used (g) and V is the volume of the solution (L).

3. Results and discussion

3.1. Synthesis and characterization of FeS_m nanocrystals

FeS_m nanoparticles have been prepared by hydrothermal treatment of thiourea formaldehyde Fe (II) complex at 170˚C for 5 h. Fig. 1(a). shows TEM images of FeS_m nanocrystals with 20 nm, the thickness and length of the FeS_m crystal was found to be 12 ± 3 and 120 ± 5 nm, respectively. The HRTEM images in Fig. 1(b) show clear fringes with interlayer spacing measured to be 0.521 ± 0.005 nm very close to lattice spacing of (0 0 1) plane of mackinawite [21]. Another lattice fringes measured with a smaller

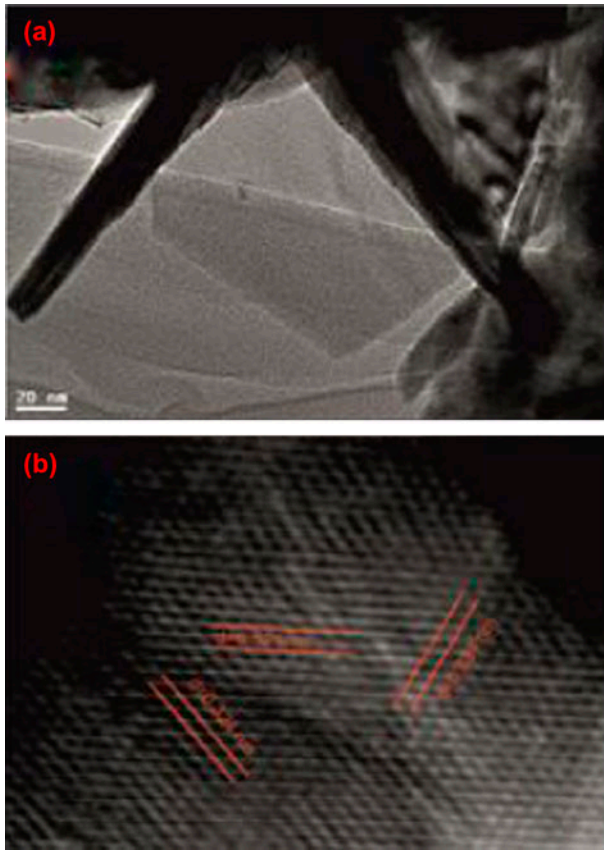

Fig. 1. (a) TEM Micrograph of synthesised FeS_m and (b) HRTEM Micrograph of synthesised FeS_m.

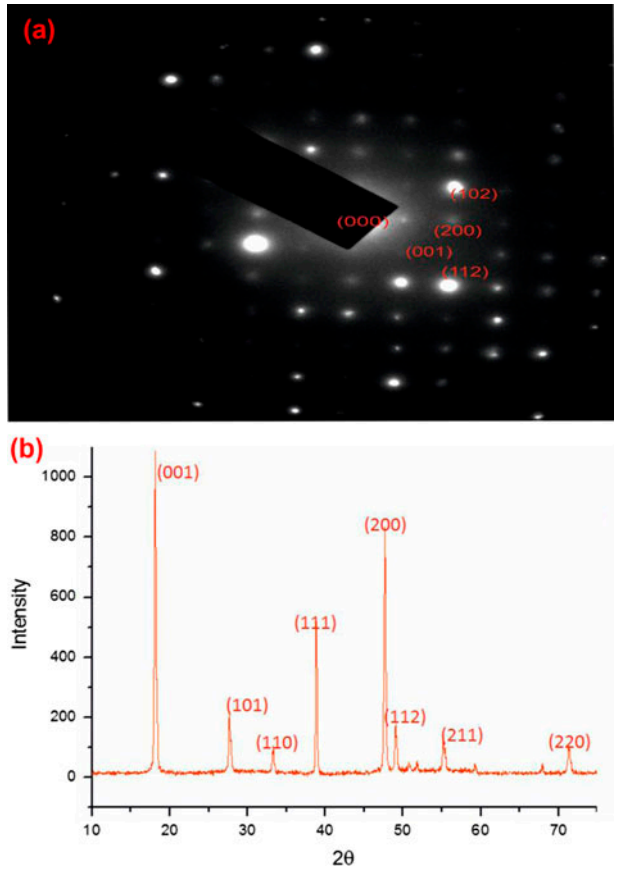

Fig. 2. (a) SAED spectrum of FeS_m and (b) XRD spectrum of FeS_m.

spacing 0.324 ± 0.005 nm corresponding to mackinawite *d*-spacing of (1 0 1) plane [22]. Fig. 2(a) shows the SAED patterns of FeS_m and clearly shows a single-crystalline structure, and the diffraction pattern indexed with *d*-spacing similar to that of crystalline mackinawite. The SAED pattern consists of broad diffuse planes, which are indicative of the small size of the particles. The diffraction point can be indexed, to the (0 0 1), (1 0 1), (2 0 0), and (1 1 2) planes, confirming the FeS_m [23,24].

The XRD pattern of the FeS_m sample shows strong and sharp diffraction peaks indicating that the product was well crystallized and presented in Fig. 2(b). All the diffraction peaks in this figure can be indexed to pure tetragonal structure FeS_m with lattice with *d*-spacing. The (0 0 1), (1 1 0), (1 0 1), (1 1 1), (1 1 2), (2 1 1), and (2 0 0) planes of FeS_m are clearly distinguishable in the pattern [25]. The broad peaks around 17.6° 2θ are corresponding to FeS_m, with intensities and positions in reasonable agreement with peaks previously reported in the conventional XRPD pattern for FeS_m [26].

3.2. Characterization of absorbed Hg(II) in the form sediment (HgS/FeS_m)

The TEM image and SAED of sediments (absorbed Hg(II) in the form HgS/FeS_m) are given in Fig. 3(a). The SAED of the sediment revealed broad diffusion rings which indicate the small size of particles. The diffraction point can be indexed to the (1 1 1), (2 2 0), (2 2 2) corresponding to HgS (cinnabar). The XRD pattern of 0.001 M Hg(II) in 0.01 M FeS_m system is given in Fig. 3(b), the peak around The peaks are corresponding to (1 0 0), (2 0 0), (2 2 0), (3 1 1) (2 2 2), and (4 0 0) which matches literature pattern for HgS [27] very well. The peak of cinnabar occurs at around 31.2° 2θ and support the adsorption of Hg(II) on FeS_m.

EDS or EDX is an analytical technique used for the elemental analysis or chemical characterization of a sample and given in Fig. 4. The corresponding EDS spectrum indicates that the FeS_m consist of Fe and S with a ratio of 1:1. The EDX spectrum of sediment (absorbed Hg(II) on FeS_m in the form of HgS) is given in Fig. 4(b); the results revealed that Hg(II) ions have been immobilized by FeS_m in the form of HgS.

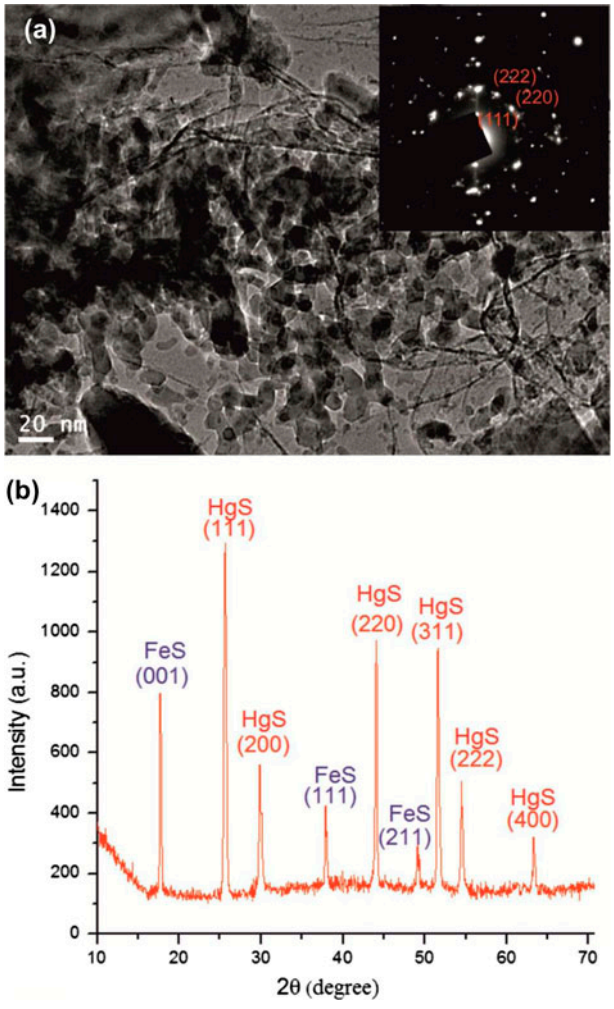

Fig. 3. (a) TEM and SAED of sediment and (b) XRD spectrum of sediment.

3.3. Recovery studies

The absorption rate of mercury was found to be depending on the time of sorption, molar ratio of Hg (II)/FeS_m, initial pH, and equilibrium pH of the solution. Fig. 5(a) illustrates the effect of time on the rate of sorption, when a fixed initial concentration of FeS_m 0.05 M and changing concentrations 0.01, 0.005, 0.001, and 0.0005 M of Hg(II) with an initial pH 5.5 was applied at room temperature. Under the given experiment with maximum concentration 0.01 M of Hg(II), within 5 h, 50–60% of the initial Hg(II) was removed from the solution, the time required to reach >95% of Hg(II) removal varied ~20 h. When the initial concentration of Hg(II) was decreased from 0.01 to 0.0005 M, the rate of absorption was increased and more than 95% removal was found within ~15 h. Another experiment in Fig. 5(b), when initial concentration (0.001 M) of FeS_m was fixed and added with 0.01, 0.005, 0.001, and 0.0005 M of Hg(II) solution at initial pH 5.5, resulting the rate of Hg(II) removal was decreased, only 8% of Hg(II) was removed with maximum initial concentration of Hg(II), when the initial concentration of Hg(II) was decreased the rate of absorption was increased and with minimum initial concentration 0.0005 M Hg(II) only 80% of Hg(II) was removed after 20 h. The decrease in percentage removal of Hg(II) is expected with decrease in FeS_m as the number of active sites decrease. Hence, lower dosage of FeS_m has negative effect on the rate of metal ion removal. Furthermore, it can be assumed that increasing initial concentration of FeS_m increases the number of collisions with Hg(II).

The actual time required to reach equilibrium could not be determined at any pH value because the Hg(II) concentration fell below the detection limit and continued to decrease over the deviation of experiment; but, based on observation, a period of 24 h should be sufficient to reach equilibrium and used for further experiments.

The maximum absorption capacity of FeS_m at initial pH 5.5 has been tested by changing the initial concentration (0.1–0.005 M) of FeS_m with fixed initial concentration (0.001 M) of Hg(II). The results revealed that 100% removal of Hg(II) was found when the concentration of Hg(II) was with 0.0125 M FeS_m. The maximum absorption capacity of FeS_m has been found with 0.080 M FeS_m, while the minimum absorption capacity was found with 0.005 M FeS_m and removed only 60% of Hg(II) from solution as shown in Fig. 6.

The relation between the initial pH of the solution and the equilibrium pH of the suspensions after adding FeS_m after 24 h for 0.01, 0.005, 0.001, and 0.0005 M initial Hg(II) concentrations. The solubility of FeS_m was depending on the pH of the solution and found that under alkaline condition, the solubility of FeS_m is lower than the solubility under acidic condition. The experiments, when a fixed initial concentration (0.05 M) of FeS_m was added with changing concentration of Hg(II), Fig. 7(a), show that the equilibrium pH increased with increase in the initial pH of the Hg(II) solution, the relationship was not proportional when the initial pH increased from 2 to 12, the equilibrium pH increases from 3 to 9 after which the data tended to be linear. The solubility of FeS_m is described by a pH-dependent reaction and a pH-independent reaction. The pH-dependent dissolution reaction can be represented by $FeS_m + 2H^+ \rightleftharpoons Fe^{2+} + H_2S$, with log K_{sp}* = −3.6 [28].

The solubility of FeS_m nanocrystals decreases with increasing pH as shown in Fig. 7(b). When the initial

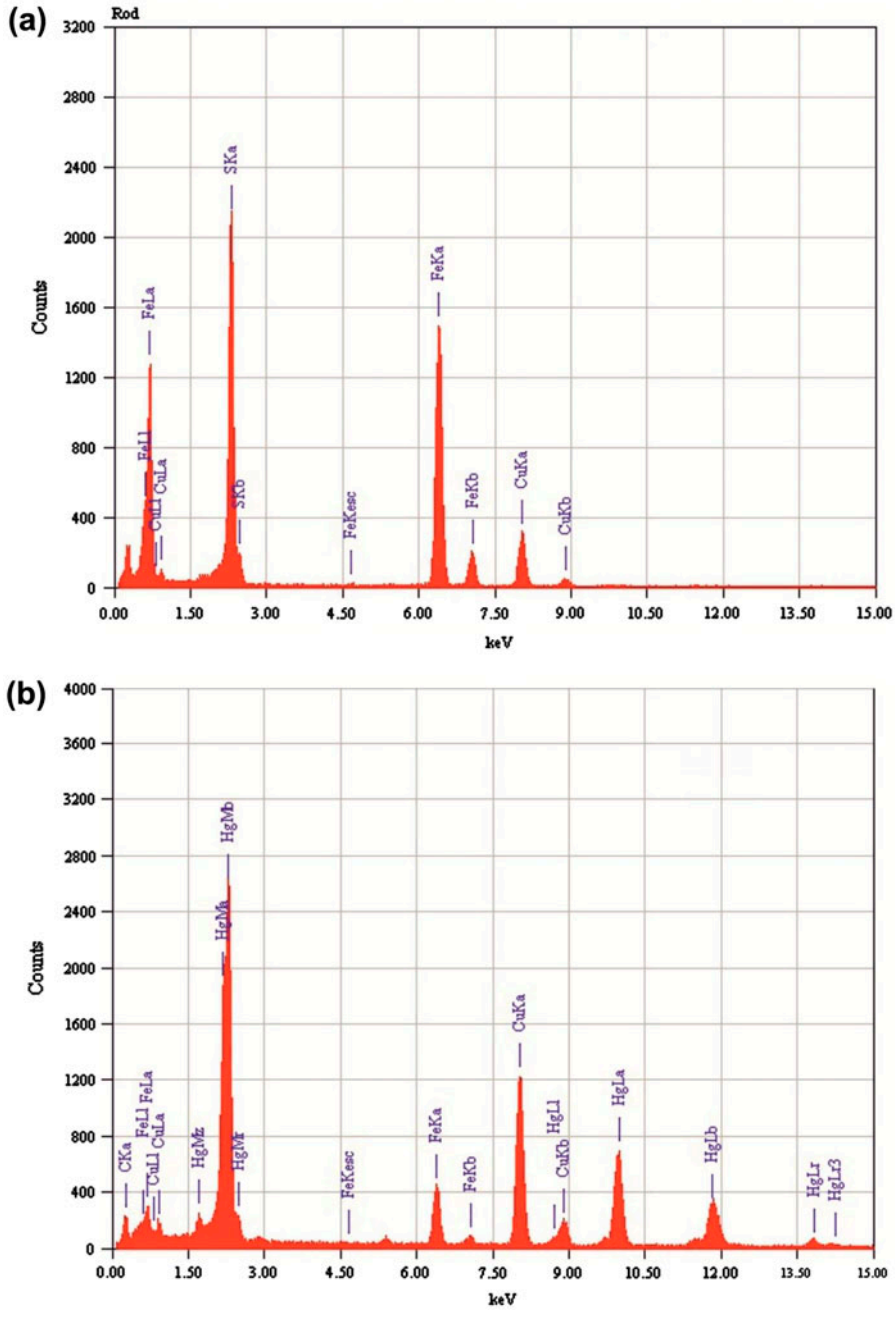

Fig. 4. EDS spectrum of (a) FeS_m and (b) HgS_m (sediment).

pH was around 2.5 (equilibrium pH < 5), loss of FeS_m was observed in the suspensions. Because of the loss of FeS_m from dissolution under low pH as expected and the sorption of Hg(II) decreased. The pH-independent dissolution reaction involves the formation of the aqueous iron sulfide cluster complex and can be represented by $FeS_m \rightleftharpoons FeS_m^0$ with log K_0 (FeS_m) = −5.7 [29].

The solubility of the FeS_m particles in acidic condition increased to immobilization of mercury. Fig. 7(c) illustrates that when (0.001 M) FeS_m was added with a changing concentration (0.01–0.0005 M) of Hg(II), the equilibrium with 0.01 M Hg(II) increased from 5 to 7 with the pH of solution increasing from 2 to 12. The same relationship was observed with the initial concentration (0.001 and 0.005 M) of Hg(II). On the other

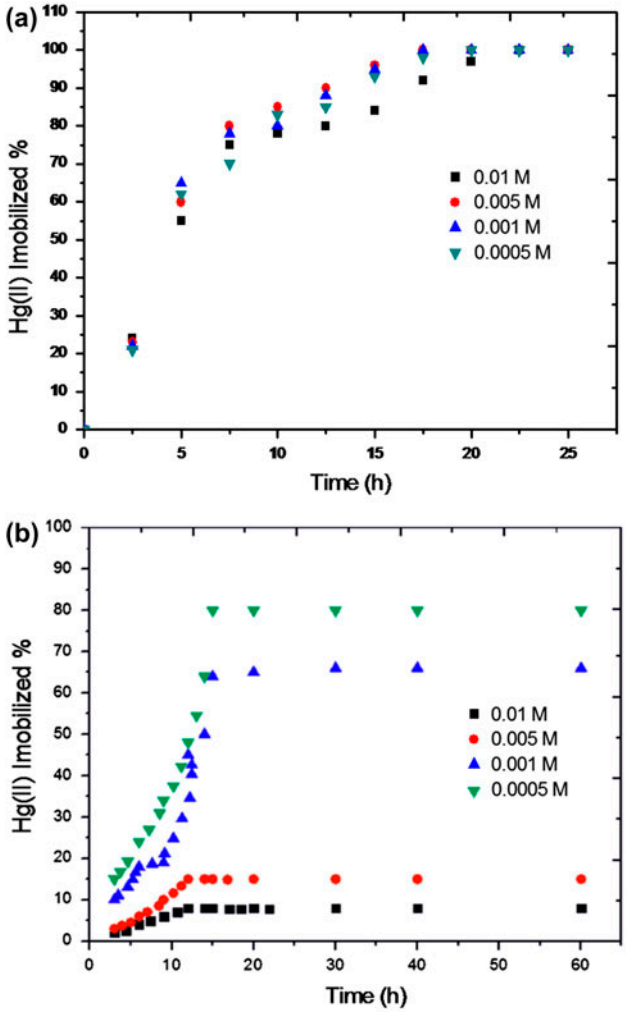

Fig. 5. Hg(II) sorption by FeS (a) with initial concentration of FeS_m 0.05 M and (b) with initial concentration of FeS_m 0.001 M.

hand, when the 100% absorption was found with (0.0005 M) concentration of Hg(II), the equilibrium pH was found near about 6 ± 0.4, when the initial pH of the solution was from 2 to 12. The absorption capacity of Hg(II) can be related to the atomic structure of the FeS_m surface. With increasing pH, the surface potential of FeS_m decreased, becoming less positive or more negative. The point of zero surface charge of FeS_m lies at pH 7.5. Under acidic conditions, it is predominantly a pH-dependent reaction.

3.4. Adsorption isotherms in a batch system

The purpose of the sorption isotherms is to reveal the specific relation between the equilibrium concentration of adsorbate in the bulk and the adsorbed amount at the surface. The most common adsorption isotherm models used to fit the equilibrium adsorption data are Langmuir Freundlich and Temkin isotherms.

The Langmuir adsorption model [30] is based on the assumption that maximum adsorption corresponds to a saturated monolayer of solute molecules on the adsorbent surface, with no lateral interaction between the adsorbed molecules. The Langmuir adsorption isotherm has been successfully used in many monolayer adsorption processes. The expression of the Langmuir model is given by Eq. (3)

$$q_e = \frac{Q_0 b C_e}{1 + b C_e} \tag{3}$$

where q_e (mg/g) and C_e (mg/L) are the amount of adsorbed adsorbate per unit mass of adsorbent and unadsorbed adsorbate concentration in solution at equilibrium, respectively. The value of Q_0 (mg/g) is the maximum amount of adsorbate per unit mass of adsorbent to form a complete monolayer on the surface bound at high C_e. and b is a constant related to the affinity of the binding sites (L/mg). The linear form of the Langmuir equation [31] is expressed as:

$$\frac{C_e}{q_e} = \frac{1}{Q_0} C_e + \frac{1}{Q_0 b} \tag{4}$$

The linear plot of specific sorption (C_e/q_e) against the equilibrium concentration (C_e) (Fig. 8) shows that the sorption of Hg(II) on FeS_m obeys the Langmuir model. The Langmuir constants Q_0 and b were determined from the slope and intercept of the plot. The low value of b obtained indicated that FeS_m has a high affinity for Hg(II). An important characteristic of the Langmuir isotherm is expressed in a dimensionless constant equilibrium parameter R_L. R_L value indicates the shape of the isotherm and is expressed by the following equation:

$$R_L = \frac{1}{[1 + b C_0]} \tag{5}$$

where b is the Langmuir constant and C_0 is the initial concentration. R_L value indicates the adsorption nature to be either unfavorable if $R_L > 1$, linear if $R_L = 1$, favorable if $0 < R_L < 1$, and irreversible if $R_L = 0$. This implies that the adsorption of Hg(II) on FeS_m is a favorable adsorption as the R_L values obtained at all initial concentrations lie between 0 and 1. This

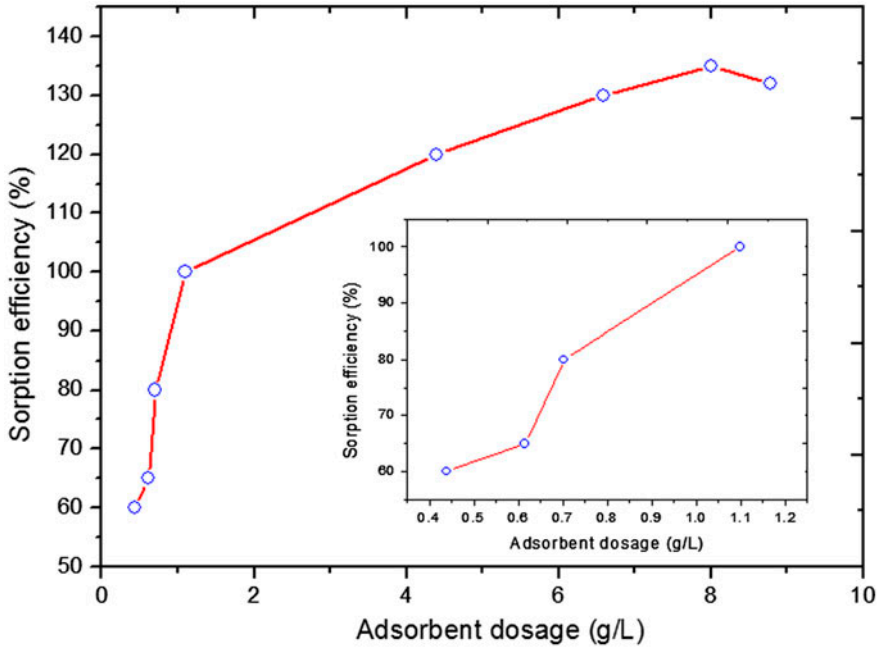

Fig. 6. Effect of the adsorbent dose on Hg(II) sorption on FeS_m (room temperature, pH 5.5).

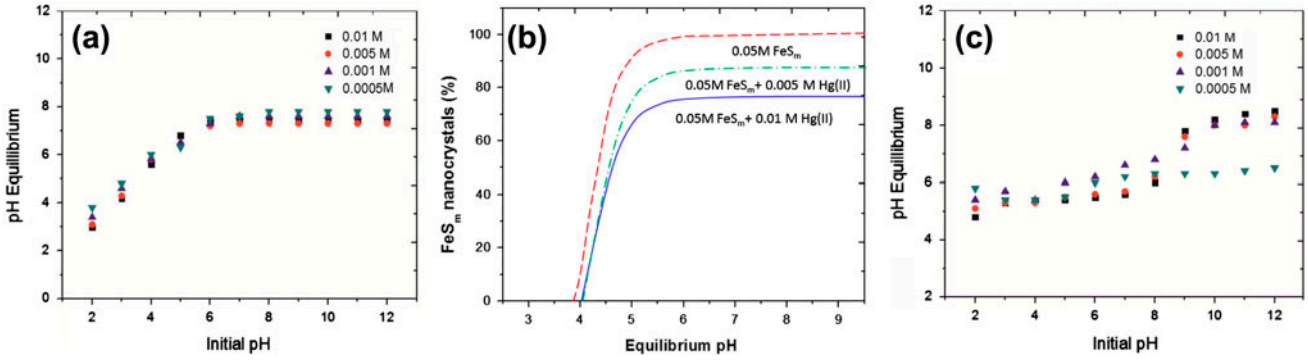

Fig. 7. Relation between equilibrium pH and initial pH (a) with initial concentration of FeS_m 0.05 M, (b) relation between FeS_m nanocrystals solubility vs. equilibrium pH, and (c) relation with initial concentration of FeS_m 0.001 M.

suggests the applicability of FeS_m for Hg(II) removal. The Langmuir isotherm parameter for Hg(II) adsorption on FeS_m nanocrystals is also in good agreement with observed behavior ($R^2 = 0.962$).

The Freundlich isotherm [32] can be applied for non-ideal sorption on heterogeneous surfaces and multilayer sorption. The Freundlich equation is expressed by the following equation:

$$q_e = K_f C_e^{1/n} \tag{6}$$

where K_f and n are Freundlich constants with K_f (mg/g (L/mg)1/n) being the sorption capacity of the adsorbent, and n giving an indication of the favorability of the sorption process. Values of $n > 1$ represent favorable adsorption condition [33,34]. To determine the constants K_f and n, the Freundlich equation can be described by the linearized form:

$$\log q_e = \log K_f + \frac{1}{n} \ln C_e \tag{7}$$

where q_e is the amount of Hg(II) adsorbed (mg g^{-1}), C_e is the equilibrium concentration of the Hg(II) (mg L^{-1}), K_f and n are the Freundlich adsorption constants which indicate the sorption capacity, and the

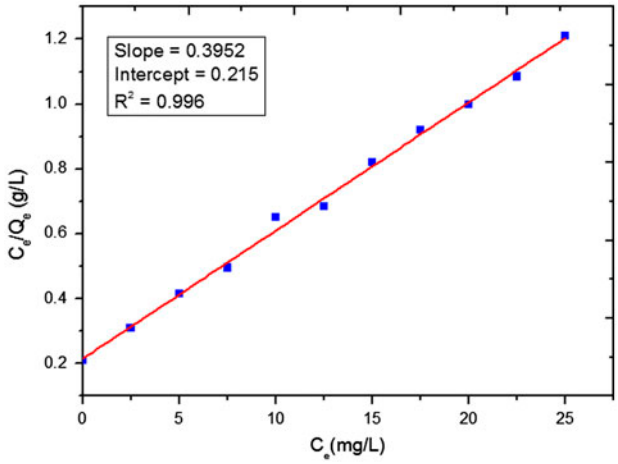

Fig. 8. Linear plot of Langmuir isotherm of Hg(II) sorption on FeS_m at room temperature.

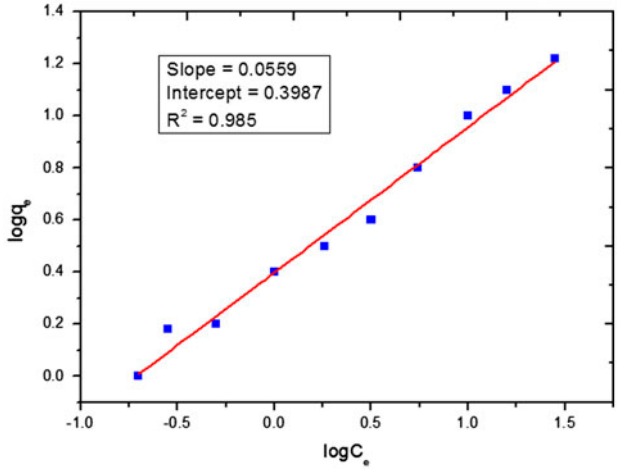

Fig. 9. Linear plot of Freundlich isotherm of Hg(II) sorption on FeS_m at room temperature.

value of K_f and n are calculated from the intercept and slope of the plot as given in Fig. 9. Values of n greater than L-type isotherms indicate the chemisorptions of Hg(II) and reflect a high affinity between adsorbate and adsorbent.

Temkin and Pyzhev considered the effects of some indirect adsorbate/adsorbate interaction on adsorption isotherms and suggested that because of these interactions, the heat of adsorption of all the molecules in the layer would decrease linearly with coverage. The Temkin isotherm has been generally applied in the following form:

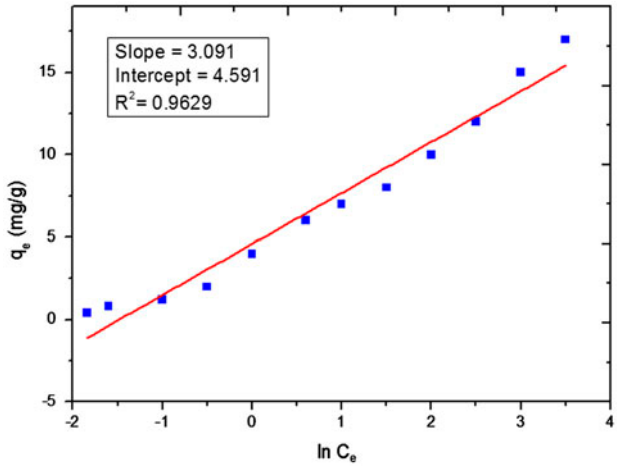

Fig. 10. Linear plot of Temkin isotherm of Hg(II) sorption on FeS_m at room temperature.

$$q_e = \left(\frac{RT}{b}\right) \ln (AC_e) \tag{8}$$

this equation can be linearized as:

$$q_e = B \ln A + B \ln C_e \tag{9}$$

where $B = RT/b$, b is the Temkin constant related to heat of sorption (J mol^{-1}); A is the Temkin isotherm constant (L g^{-1}), R is the gas constant (8.314 J mol^{-1} K^{-1} J/mol K), and T is the absolute temperature (K).

Fig. 10 shows the linear plot of Temkin isotherm of Hg(II) on FeS_m at 30°C. The constants A and B are calculated from the intercept and slope of the plot. The Temkin adsorption isotherm achieved very good fit for the adsorption data, with correlation coefficients ($R^2 = 0.996$) indicating chemisorption of the Hg(II) onto FeS_m nanocrystal. On the basis of earlier findings, we concluded that the adsorption of Hg(II) onto FeS_m nanocrystals was entirely a chemisorptions process.

4. Conclusion

Stabilized mackinawite FeS_m nanocrystals were successfully prepared by single precursor polymer metal complexes. The synthesized nanocrystals have been characterized by XRD and electron microscopy. The absorption study shows that FeS_m nanocrystals are highly effective to immobilized Hg(II) in aqueous solution under both aerobic and anaerobic condition. The results revealed that 100% removal of Hg(II) was found when the concentration of Hg(II) was with

0.0125 M FeS_m. The maximum absorption capacity of FeS_m has been found with 0.080 M FeS_m. The adsorption isotherm was well fitted with the Langmuir and Freundlich Temkin and Pyzhev models. In this study, we have synthesised stabilized FeS_m nanoparticles, but all the reactions and adsorption studies have been carried out in nitrogen environment.

Acknowledgments

The authors extend their appreciation to the Deanship of Scientific Research at King Saud University for funding this work through research group no RG-1435-007.

References

[1] W.G. Shipp, R.A. Zierenberg, Pathways of acid mine drainage to Clear Lake: Implications for mercury cycling, Ecol. Appl. 18(Suppl 8) (2008) 29–54.
[2] D.M. Manohar, K. Anoop Krishnan, T.S. Anirudhan, Removal of mercury(II) from aqueous solutions and chlor-alkali industry wastewater using 2-mercaptobenzimidazole-clay, Water Res. 36 (2002) 1609–1619.
[3] B.S. Inbaraj, J.S. Wang, B. Stephen, J.F. Lu, F.Y. Siao, B.H. Chen, Adsorption of toxic mercury(II) by an extracellular biopolymer poly(cglutamic acid), Bioresour. Technol. 100 (2009) 200–207.
[4] B.S. Inbaraj, N. Sulochana, Mercury adsorption on a carbon sorbent derived from fruit shell of *Terminalia catappa*, J. Hazard. Mater. 133 (2006) 283–290.
[5] H. Yavuz, A. Denizli, H. Güngüneş, M. Safarikova, I. Safarik, Biosorption of mercury on magnetically modified yeast cells, Sep. Purif. Technol. 52 (2006) 253–260.
[6] M.M. Rao, D.H.K. Kumar Reddy, P. Venkateswarlu, K. Seshaiah, Removal of mercury from aqueous solutions using activated carbon prepared from agricultural by-product/waste, J. Environ. Manage. 90 (2009) 634–643.
[7] M. Zabihi, A. Haghighi Asl, A. Ahmadpour, Studies on adsorption of mercury from aqueous solution on activated carbons prepared from walnut shell, J. Hazard. Mater. 174 (2010) 251–256.
[8] L. Axe, P.R. Anderson, Sr diffusion and reaction within Fe oxides: Evaluation of the rate-limiting mechanism for sorption, J. Colloid Interface Sci. 175 (1995) 157–165.
[9] B.C. Bostick, S. Fendorf, G.R. Helz, Differential adsorption of molybdate and tetrathiomolybdate on pyrite (FeS_2), Environ. Sci. Technol. 37 (2003) 285–291.
[10] J.W. Patterson, Industrial wastewater treatment technology, Butterworth, Boston, MA, 1985, pp. 203–214.
[11] B.C. Bostick, S. Fendorf, Arsenite sorption on troilite (FeS) and pyrite (FeS_2), Geochim. Cosmochim. Acta 67 (2003) 909–921.
[12] X. Zhong, H. Feng, Z. Dongye, B. Mark, Immobilization of mercury in sediment using stabilized iron sulfide nanoparticles, Water Res. 43 (2009) 5171–5179.
[13] W. Hongtao, A. Keller, L. Fengting, Natural organic matter removal by adsorption onto carbonaceous nanoparticles and coagulation, J. Environ. Eng. 136 (2010) 1075–1081.
[14] L. Xiaogang, Z. Lina, High effective adsorption of organic dyes on magnetic cellulose beads entrapping activated carbon, J. Hazard. Mater. 171 (2009) 340–347.
[15] D.K. Tiwari, J. Behari, P. Sen, Application of nanoparticles in waste water treatment, World Appl. Sci. 3 (2008) 417–423.
[16] X. Qu, P.J. Alvarez, Q. Li, Applications of nanotechnology in water and wastewater treatment, Water Res. 47(12) (2013) 931–946.
[17] S.K. Brar, M. Verma, R.D. Tyagi, R.Y. Surampalli, Engineered nanoparticles in wastewater and wastewater sludge—Evidence and impacts, Waste Manage. 30 (3) (2010) 504–520.
[18] J.M. Moore, W.H. Ficklin, C. Johns, Partitioning of arsenic and metals in reducing sulfidic sediments, Environ. Sci. Technol. 22 (1988) 432–437.
[19] A. Tansir, K. Vikrant, N. Nahid, S, Synthesis, characterization and antimicrobial activity of transition metal chelated thiourea-formaldehyde resin, Polym. Int. 55 (2006) 1398–1406.
[20] X. Zhong, H. Feng, Z. Dongye, O.B. Mark, Immobilization of mercury in sediment using stabilized iron sulfide nanoparticles, Water Res. 43 (2009) 5171–5179.
[21] O. Hiroaki, R. David, High resolution transmission electron microscopic study of synthetic nanocrystalline mackinawite, Earth Planet. Sci. Lett. 241 (2006) 227–233.
[22] M. Wolthers, S.J. Van, D. Rickard, The structure of disordered mackinawite, Am. Mineral. 88 (2003) 2007–2015.
[23] A.R. Lennie, K.E.R. England, D.J. Vaughan, Transformation of synthetic mackinawite to hexagonal pyrrhotite: A kinetic study, Am. Mineral. 80 (1985) 960–967.
[24] A.R. Lennie, K.E.R. England, D.J. Vaughan, Transformation of mackinawite to greigite: An in situ X-ray powder diffraction and transmission electron microscope study, Am. Mineral. 82 (1997) 302–309.
[25] Z. Zhang, F. Zhou, F.J. Lavernia, On the analysis of grain size in bulk nanocrystalline materials via x-ray diffraction, Metall. Mater. Trans. A 34 (2003) 1349–1355.
[26] M. Wolthers, S.J. Van der Gaast, D. Rickard, The structure of disordered mackinawite, Am. Mineral. 88 (2003) 2007–2015.
[27] Joint Committee on Powder Diffraction Standards (JCPDS), File No. 6-261.
[28] W. Davison, The solubility of iron sulphides in synthetic and natural waters at ambient temperature, Aquat. Sci. 53 (1991) 309–329.
[29] M. Macnaugh, R.O. James, Adsorption of aqueous mercury (II) complexes at oxide–water interface, J. Colloid Interface Sci. 47 (1974) 431–440.
[30] J. Eastoe, J.S. Dalton, Dynamic surface tension and adsorption mechanisms of surfactants at the air water interface, Adv. Colloid Interface Sci. 85 (2000) 103–144.
[31] K. Saltalı, A. Sarı, M. Aydın, Removal of ammonium ion from aqueous solution by natural Turkish (Yıldızeli) zeolite for environmental quality, J. Hazard. Mater. 141 (2007) 258–263.
[32] H. Freundlich, Uber die adsorption in losungen (Adsorption in solution), Z. Phys. Chem. 57 (1906) 384–470.
[33] Y.S. Ho, G. McKay, Sorption of dye from aqueous solution by peat, Chem. Eng. J. 70 (1998) 115–124.
[34] M.J. Temkin, V. Pyzhev, Recent modifications to Langmuir isotherms, Acta Physiochim., URSS 12 (1940) 217–222.